Generation of Functional Images of The Brain Trapping Constant for α-[^{11}C]Methyl-L-Tryptophan Using Constrained Linear Regression

Y. Kumakura, J. Natsume, P.-J. Toussaint, A. Nakai, P. Rosa-Neto, E. Meyer and M. Diksic*

Department of Neurology and Neurosurgery, and Montreal Neurological Institute, McGill University, Montreal, QC, Canada

Abstract: The main objective of described work was a generation of the functional images of the brain trapping constant (K*; μL/g/min) of α-methyl-L-tryptophan, an index of 5-HT synthesis, which under some assumptions is related to the serotonin synthesis. Comparisons of the regional K* calculated by the Patlak approximation, non-linear fitting and the linearized form of the non-linear operational equation were made and discussed. In addition a contrast between the white and gray matter K* values was evaluated by different methods. Results presented suggest that the linearized form of the operational equation yields the best gray to white matter contrast. It was also shown that with this calculation approach, as was shown before for the Patlak approximation, the use of the venous sinus-venous blood normalized input function instead of the arterial input function is satisfactory. Also results show that the error of the K* estimates is smaller than those in the Patlak estimates, when the linearized solution of the model equation is used. Simulation results indicate that the coefficient of variation for K* is smaller than some errors for the equation parameters.

Keywords: Tracer kinetics; human brain imaging; α-methyl-L-tryptophan; positron emission tomography.

INTRODUCTION

5-Hydroxytryptamine (5-HT, serotonin) is a neurotransmitter widely distributed in the brain with diffuse projections throughout the brain [1]. It has been suggested that 5-HT is involved in the pathophysiology of several affective disorders. Pharmacological treatments influencing the serotonergic system have shown that sleep, eating, mood and impulsive behaviour among others are modulated by 5-HT [2-4]. These influences are observed not only in normal subjects but also in patients suffering from affective disorders. Therefore, the development of an in-vivo method to assess 5-HT synthesis, one of the most important factors of serotonergic neurotransmission [5], in human brain, is of great importance and should help us in getting a better understanding of the alterations in the brain serotonergic neurotransmission in different affective disorders.

α-Methyl-L-tryptophan (α-MTrp) is an analog of tryptophan (Trp) which traces the Trp conversion into 5-HT, and the brain trapping of α-MTrp (K*; μL/g/min) is highly correlated with Trp conversion into 5-HT [6]. Numerous autoradiographic experiments in rodents were performed to validate α-MTrp as a radioactive tracer to measure 5-HT synthesis *in vivo* [7-10]. The experimental data suggest that the tissue trapping of α-MTrp correlates with the constant for Trp conversion to 5-HT in the brain, while neither Trp incorporation into proteins nor the Trp transport through the blood brain barrier correlate with the trapping constant for α-MTrp [6]. Labelling α-MTrp with a positron emitter made it possible to visualize α-MTrp trapping and use it as an index of 5-HT synthesis in living mammalian brain with positron emission tomography (PET) [9,11-15]. In normal subjects, and probably in many subjects with affective disorders in which alternative metabolic pathway of Trp is not activated this alternative patway can be disregarded (e.g. kinurinic/quinolinic pathways; [16]). Under the assumptions discussed in our reviews [8,9], the trapping constant of α-MTrp can be used as an index of 5-HT synthesis because it is highly correlated to the conversion of Trp into 5-HT [6]. To reduce the invasiveness of arterial blood sampling required in quantitative PET studies, an alternative, less-invasive, method was developed by combining the venous plasma time-activity curve (TAC) and the TAC of the venous sinus obtained from the dynamic PET images [17]. We [11,13,17,18] and others [12,16] have been using the Patlak method for α-MTrp PET studies, but this method might introduce a bias, because there is some uncertainty as to which part of the Patlak plot should be assumed to be linear [12,17]. Since the slope of the linear regression line is determined by a particular, often somewhat arbitrary, segment of the Patlak plot, the estimates of the brain trapping constant K* (ml/g/min) from this particular segment of the TAC are biased to some extent [12,17]. However, if the analysis is done consistently, between and within group comparisons are not greatly affected.

To overcome some of the problems of the Patlak plot in the α-MTrp TAC analysis, we are proposing the adaptation of a linear solution of the three-compartment (two-tissue compartments) model described by Blomqvist [19].

*Address correspondence to this author at the Montreal Neurological Institute, McGill University, 3801 University Street, Montreal, Quebec, H3A 2B4, Canada; Tel: +1-514-398-8526; Fax: +1-514-398-8195;
E-mail: Mirko.Diksic@mcgill.ca

1874-3471/11

The investigation described here had four goals: **1)** utilizing a less-invasive input function for the linearized solution of the model equation; **2)** generating a whole brain image of the trapping constant K* [=K1k3/(k2+k3)]; **3)** evaluating the bias generated by the pixel-by-pixel calculation of the K* image, and **4)** comparing the K* images of the linear solution to those of the Patlak method in order to assess specifically the gray to white matter contrast.

MATERIAL AND METHODS

Twelve male and nine female healthy volunteers, aged from 20 to 65 (Mean± SD: 34.6±14.2), were used in this study. Three of these subjects, those with both arterial and venous blood sampling, were used in our previous publication [17] in which arterial and venous-sinus-derived input functions were compared. The study described here was approved by the Research and Ethics Committee of the Montreal Neurological Institute and Hospital, and the Institutional Review Board of McGill University. All subjects provided written informed consent to participate in the study. The absence of any medical, neurological, and psychiatric history (including alcohol and drug abuse) was assessed by subject's history, physical examination, routine blood tests, urine toxicology and electrocardiogram. Psychiatric evaluation was done using the Structural Clinical Interview for the Diagnostic and Statistical Manual of Mental Disorders, revised (DSM-III-R), non-patient version. Exclusion criteria included evidence of a past or present axis-I or -II DSM-III-R diagnosis in the subjects, or in their first-degree relatives, or any significant medical illness.

The radiopharmaceutical α-[^{11}C]MTrp was prepared as previously described [20]. Injected dose and mass were less than 0.56 GBq (15 mCi) and 15μg, respectively.

All PET studies were carried out in the morning after an overnight fast (water was allowed ad libitum). On the day before the PET study, all subjects were fed a standard low-protein diet to minimize inter individual variability of plasma amino acid concentrations. PET data were acquired by an ECAT EXACT HR+ scanner (Siemens/CTI, Knoxville, TN, USA). This scanner produces 63 slices with an intrinsic resolution of 5.0 x 5.0 x 5.0 mm full width at half maximum (FWHM) in 3D mode. A 10-minute transmission scan was completed before radiotracer injection. The dose of α-[^{11}C] MTrp was injected manually intravenously over 2 minutes. All emission data were collected in the 3D mode for 60 minutes as twenty six consecutive frames of increasing duration (6x30 seconds, 7x60 seconds, 5x2 minutes 8x5 minutes) and then reconstructed to 128x128-matrix planes using a Hanning filter of 8.1 mm FWHM in the transaxial direction, yielding images with a FWHM resolution of about 9.5 mm.

After radiotracer injection, blood samples were collected from an antecubital vein every 15 to 30 seconds in the first 2 minutes, every one minute during the next 3 minutes, every 3 to 5 minutes up to 20 minutes, and every 10 minutes for the rest of the scan. Three subjects underwent arterial blood sampling from a radial artery simultaneously. After centrifugation (10,000 g for 1 min), plasma was collected in 200 μL aliquots, and radioactivity was measured in a well-gamma counter (Canberra Industries, CT). During the PET scan, five additional venous blood samples were drawn for measurements of free and total plasma concentrations of tryptophan by high-performance liquid chromatography (HPLC).

The input function, without arterial blood sampling, was constructed as described and tested before, where also several examples of this combined input functions are given [17]. Briefly, this input function consists of the venous sinus TAC taken from the dynamic PET images for the first 20 min after tracer injection and the venous plasma TAC after 20 min up to the end of the scan. To extract the venous sinus TAC, a small ROI was drawn through 3-4 slices, including "torcular herophili" (the confluence of the straight and transverse sinuses located posterior in the occipital region). The initial TAC (20 min) from the venous sinus was normalized to the venous plasma radioactivity at 20 minutes to generate an input function for the whole PET scan period. The input function (Ca(t), Bq/mL) was fitted to a sum of three exponentials for the segment from the peak point to the end to obtain a smoothed input function in an attempt to reduce the influence of errors in the plasma sampling.

Image Acquisition and Segmentation procedures

Magnetic resonance imaging (MRI) scans were acquired by a 1.5-T Gyroscan (Philips Medical Systems, Eindhoven, the Netherlands) using a T1-weighted fast field echo (repetition time=18 msec, echo time=10msec, 1 acquisition average pulse sequence, flip angle=30 degrees, matrix size=256x256, field of view=256x256, thickness=1mm), following a scout view of axial, sagittal, and coronal planes (localizer). Approximately 170 isotropic images with a voxel size of 1x1x1 mm were acquired. Some subjects were scanned by a 1.5 T Siemens Vision Magnetom (Erlangen, Germany) using a T1-weighted 3D gradient echo sequence (TR 18 ms, TE 10 ms, 1 signal average, flip angle 30 degrees, matrix 256x256, FOV 250, thickness 1mm). All of the MRI images underwent automated correction for intensity non-uniformity caused by radiofrequency inhomogeneity [21].

Image analysis was performed on a Silicon Graphics workstation (Mountain View, CA) with software libraries developed at the Montreal Neurological Institute [21-24].

Forty-four regions of interest (ROI-s) were segmented in the native MRI space, but only the gray matter regions (fourteen ROI-s both on left and right sides) and the brain stem ROI were used in this study. To extract volumes of individual brain structures objectively, an automatic MRI segmentation program developed at the Montreal Neurological Institute was used [21-24]. The program, ANIMAL+INSECT (Automatic Nonlinear Image Matching and Anatomical Labeling plus Intensity Normalized Stereotaxic Environment for Classification of Tissues), employs a nonlinear registration procedure, a pre-labeled target volume on the referent MRI volumetric data, and tissue classification into white matter, gray matter and CSF space, using an artificial neural network algorithm. It provides segmented ROI-s on each subject's native MRI volume data, corresponding to a set of targeted anatomical structures. Some minor segmentation errors were repaired by manual pixel painting and erasing. Finally, all of the segmented ROI-s were reviewed by a qualified neurologist, and the ROI-s for the gray matter structures (amy_l, amy_r, cing_l, cing_r, CN_l, CN_r, DG_l, DG_r, for_l, for_r, GM_lf, GM_lo, GM_lp, GM_rf, GM_ro,

GM_rp, hip_l, hip_r, ins_l, ins_r, mtmp_l, mtmp_r, PuGP_l, PuGP_r, stem, Th_l, Th_r, tmp_l, tmp_r) were used in the further analysis.

For MRI-PET registration, MRI images and segmented ROI-s were co-registered and resample individually to PET images in native space [24]. To generate a tissue activity image in native space, the last 8 frames of the dynamic PET images were summed up.

The kinetic model of α-MTrp is constructed on the basis of experimental data supporting transfer of the tracer from plasma through the precursor pool into an irreversible compartment [6-8, 25]. There is no direct communication for the tracer between the irreversible compartment and the plasma compartment. It was shown before that adding an irreversible compartment (second tissue compartment assumed to be irreversible during the study) in the structure improves significantly the goodness of fit [8].

In Fig. (**1**), the model is illustrated by using rate constants in units of min^{-1}, except for K1*(mL/g/min). K1* is the product of the first order rate constant k1* (min^{-1}) and the plasma volume (mL/g) from which the tracer is extracted. The rate constant k2* (min^{-1}) describes the tracer transfer from the precursor pool to plasma, while k3* (min^{-1}) characterizes the tracer transfer from the precursor pool to the irreversible pool in the model. K* =K1*k3* /(k2* +k3*) (mL/g/min) is defined as the constant of trapping of α-MTrp in terms of the three rate constants of this kinetic compartmental model. The transfer of the tracer can be described by a multilinear solution to the set of differential equations describing tracer movement in a three compartment model [19].

Here, Ci(T) [Bq/g] is the instantaneous tissue tracer concentration, and Cp(t) [Bq/mL] is the plasma tracer concentration as a function of time. When this linear equation is applied to each frame end time (0, Ti; i =1,2 , where n (number of frames) is >2) in the PET acquisition, a set of linear equations with three macro-parameters, a=K1, b=K1Ak3, and c=k2+k3, is obtained. This set of equations can be solved by standard methods, and the values of the macro parameters a, b, and c obtained. To avoid non-physiological solutions, non-negative constraints were added to the macro-parameters a, b, and c. These macro-parameters should be non-negative, because all of the rate constants, K1, k2 and k3, should by definition be positive. From a, b, and c the brain trapping constant K*; mL/g/min was calculated as b/c. In the fitting BV (blood volume) was fixed to zero or a value of 0.03 (3% blood volume).

The Patlak method does not require any assumption on either number or configuration of the kinetic compartments. This method allows graphical determination of the unidirectional uptake (Ki) of α-MTrp as the slope of the regression line, which accounts for net transport (irreversible trapping) from the blood plasma into the brain. The estimates were calculated using the following equation:

$$Ci(T) = K1\int_0^T Cp(t)dt + K1k3\int_0^T \int_0^t Cp(v)dvdt - (k2 + k3)[\int_0^T Ci(t)dt - BV\int_0^T Cp(t)dt] + BVCp(T) \quad (1)$$

DV(T) (Eq. 2) represents tissue volume of distribution for the tracer, Ki can be assumed, in the case of two tissue compartment model, to be equal to K* [K1*k3*/(k2*+k3*)].

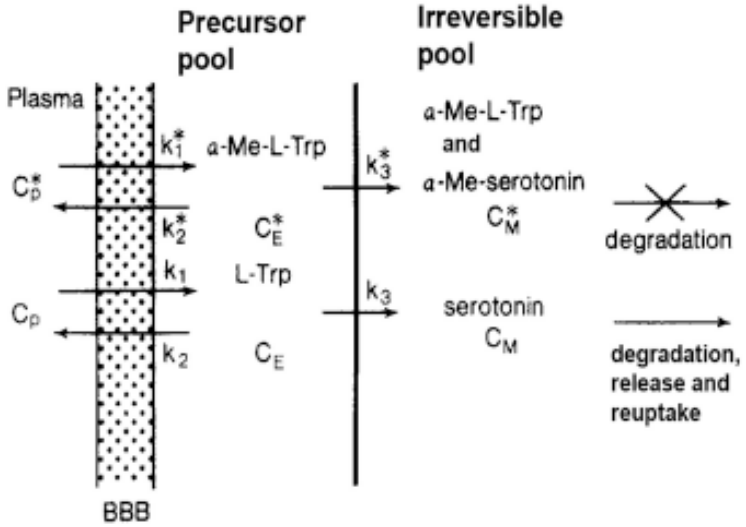

Fig. (1). A schematic representation of a biological model for α-MTrp depicting metabolic pathways of Trp and α-MTrp (tracer). The rate constants with an asterisk are those for the tracer and the ones without an asterisk are for Trp (e.g. k_1 and k_1^* are the first order rate constants for Trp and labelled α-MTrp describing transport through the blood-brain barrier (BBB). The rate constants responsible for the movement of the tracer between different compartments are assumed to be the first-order rate constants and have units of reciprocal time except K_1, which has units of mL/g/min. This constant is actualy a product of the k_1^* (min^{-1}) and the plasma volume in a gram of brain (ml/g). The rate constant k2* describes the tracer movement from the precursor pool to plasma, while k3* characterizes the tracer movement from the precursor pool to the irreversible pool of brain tissue. K*(=K_1*k_3* /k_2* +k_3*) is defined as the constant of the irreversible trapping. Adapted from Diksic and Young, 2000.

Vapp represents the apparent distribution volume of the tracer. In the Patlak method, the vascular space (BV) is implicitly included into Vapp which is an adjustable parameter.

$$DV(T) = \frac{Ci(T)}{Cp(T)} = Ki \cdot \frac{\int_0^T Cp(t)dt}{Cp(T)} + Vapp \quad (2)$$

Comparison 1: *Evaluation of different input functions*. In the first comparison, K* maps were generated by pixel-by-pixel calculation using Eq. 1 (multi linear equation). Two kinds of maps were obtained: one using the arterial input functions (K^*_a), and a second one using the less-invasive (sinus-venous blood normalized) input function (K^*_s). The values obtained by the two approaches were compared. The K^*_a and K^*_s maps were compared by segmentation in the above mentioned ROIs and the K* values from the ROIs were extracted. Additionally, the K^*_s (sinus-venous blood normalized) and K^*_a (arterial) values were calculated for the TAC-s from those ROI using arterial and the less-invasive (combination of sinus and venous plasma; [17] input functions. Likewise, the maps of the macro parameters (a, b, and c) were also generated using two different input functions allowing the comparison of results obtained with the arterial and the less-invasive input functions. The ROI values of the macro parameters (a, b, and c) obtained with the less-invasive and the arterial input functions were compared in addition to the main comparison of the parameter of interest, K^*_a and K^*_s. In addition the ratios of parameters a, b, and c, and K* calculated with the sinus-venous blood normalized and arterial input functions were calculated, to asses the bias of different input function.

Comparison 2: *K* from pixel-by-pixel and ROI fitting using venous-venous sinus input function* In this comparison, two sets of K* estimates were obtained using the less-invasive input function and the linear solution (Eq. 1). Twenty-one normal subjects were included in this comparison. For the first set of K*-values, the K*-maps were used to extract K* for different ROIs (K*p). The second set of K* was obtained from the TACs for the ROIs obtained from the dynamic PET images and the linear solution (Eq. 1) to obtain K* estimates (K*r). The ratios of K*p/K*r were calculated for 40 brain structures on the MRI-based segmented ROIs to evaluate the difference between K*p and K*r.

Comparison 3: *K* from the Patlak and the Blomqvist method for the whole brain*. For the third comparison, both K*-maps by the linear solution (Eq. 1) and Ki maps by the Patlak method (Eq. 2) were generated using the less-invasive input function. From this comparison we could determine which of the two trapping constant maps, the Ki-map by the Patlak method or the K* map by the linear solution, showed better contrast between gray and white matter. This ratio is assumed to reflect 5-HT synthesis in the brain, because the synthesis occurs in the gray matter serotonergic neurons. This contrast (gray-white matter ratio) was calculated for the frontal, temporal, parietal and occipital lobes from both K*- and Ki- maps (Table **3**). These contrast ratios were compared by the paired t-test for the structures of the left and right half of the brain in twenty-one normal subjects. The gray matter ROIs were also drawn to obtain the mean values of K*, and

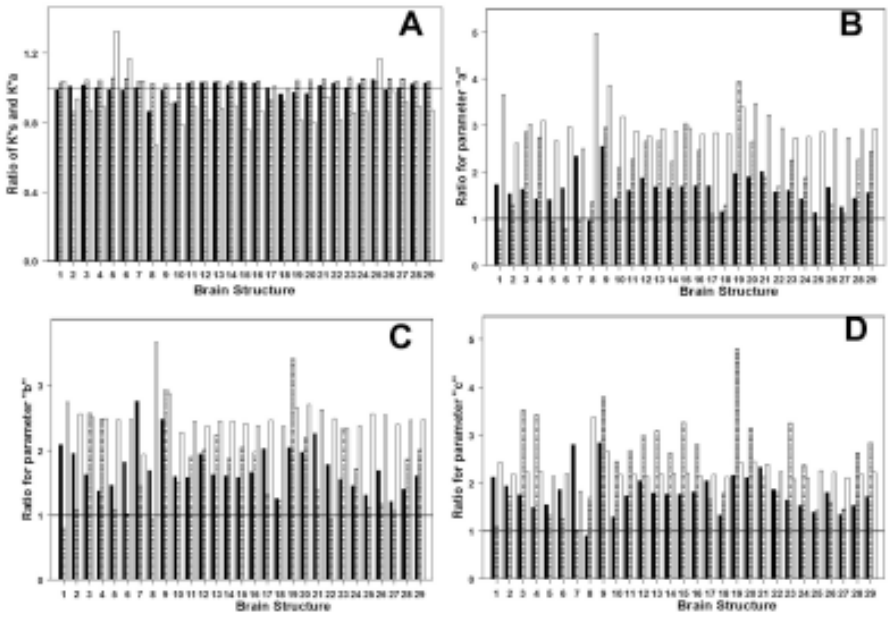

Fig. (2). A graphical presentation of the ratios of different model parameters calculated by using venous-sinus and arterial input functions. The bars represent the values in three different subjects for 29 brain regions. The brain regions abbreviations are defined in the list of abbreviations and the brain regions presented here are as follows: 1=amy_l; 2=amy_r; 3=cing_l; 4=cing_r; 5=CN_l; 6=CN_r; 7=DG_l; 8=DG_r; 9=for_l; 10=for_r; 11=GM_lf; 12=GM_lo; 13=GM_lp; 14=GM_rf; 15=GM_ro; 16=GM_rp; 17=hip_l; 18=hip_r; 19=ins_l; 20=ins_r; 21=mtmp_l; 22=mtmp_r; 23=PuGP_l; 24=PuGP_r; 25=stem; 26=Th_l; 27=Th_r; 28=tmp_l; 29=tmp_r. In the insert A the ratios between K^*_s and K^*_a are shown with the line at the ratio of 1. In the insert B the ratios between model parameters a calculated with the venous-sinus and arterial input functions are given. In the inserts C and D the ratios between model parameters b and c, respectively, calculated with the venous-sinus and arterial input functions are given. In all inserts a line at the ratio of 1 is shown.

Table 1. Mean Volumes of MRI-Based Segmentation of 44 Brain Structures for 21 Subjects

Name of Region	Abbreviation	Mean (mL)	SD (mL)
amygdala(left)	amy_l	0.60	0.08
amygdala(right)	amy_r	0.62	0.06
cingulate (left)	cing_l	4.11	1.44
cingulate (right)	cing_r	2.84	0.90
caudate nucleus (left)	CN_l	1.54	0.24
caudate nucleus (right)	CN_r	1.65	0.25
hypothalamus and other nucleus** (left)	DG_l	0.32	0.03
hypothalamus and other nucleus **(right)	DG_r	0.32	0.02
fornix (right)	for_l	0.58	0.17
fornix (right)	for_r	0.54	0.15
gray matter (left frontal)	GM_lf	36.41	12.26
gray matter (left occipital)	GM_lo	20.42	6.03
gray matter (left parietal)	GM_lp	20.30	4.71
gray matter (right frontal)	GM_rf	35.89	12.24
gray matter (right occipital)	GM_ro	19.39	6.21
gray matter (right parietal)	GM_rp	20.03	4.19
hippocampus (left)	hip_l	0.82	0.10
hippocampus (right)	hip_r	0.88	0.11
insula (left)	ins_l	3.47	0.41
insula (right)	ins_r	3.27	0.51
mesial temporal lobe*, left	mtmp_l	2.92	0.99
mesial temporal lobe*, right	mtmp_r	2.70	0.98
putamen, globus palladus (left)	PuGP_l	2.10	0.27
putamen, globus palladus (right)	PuGP_r	2.15	0.24
brain stem	stem	12.36	2.04
thalamus (left)	Th_l	2.93	0.39
thalamus (right)	Th_r	2.77	0.40
lateral temporal lobe gray matter (left)	tmp_l	28.44	4.06
lateral temporal lobe gray matter (right)	tmp_r	30.32	5.77

*mesial temporal lobe, including hippocampus, amygdala, and parahippocampal area.
**hypothalamus, subthalamic nucleus, and nucleus accumbens.

the coefficient of variation for K* and Ki, calculated from the respective K* map.

Simulation

All fittings of experimental data to model equations are influenced by errors in measured data points (e.g. errors in the plasma input functions and the tissue tracer concentrations measured by PET). Tissue time activity curves (TAC) are usually obtained from PET frames of variable duration; short frames at the beginning and longer later on. The plasma input function is usually fitted to a sum of exponentials after a peak and a linear function to the peak which results in a smooth input function whith a large number of data points. Because of this, the influence of measurement error in the input function on the estimation of the model parameters is much less pronounced (data not presented) and was not described here. An influence of different level of errors in the TACs on the estimation of the model parameters was

Table 2. Differences Between Pixel-Based (K*p) and ROI-Based (K*r) Calculations Using the Linear Solution and Less-Invasive Input Function for 21 Normal Control Subjects[1]

	K*r[2]		K*p[3]		% of Mean Change
brain region[4]	mean±SD	COV	mean±SD	COV	(K*r-K*p)/K*r (%)
amy_l	6.37±3.02	47	5.98±2.86	48	6.19
amy_r	6.05±2.54	42	5.66±2.54	45	6.36
cing_l	6.90±2.36	34	6.55 ±2.39	36	5.04
cing_r	7.20±2.55	35	6.86±2.51	37	4.67
CN_l	6.94±2.58	37	6.59±2.61	40	5.16
CN_r	7.02±2.42	35	6.62±2.51	38	5.66
DG_l	6.25±2.64	42	5.85±2.57	44	6.49
DG_r	6.27±2.77	44	5.92±2.65	45	5.49
for_l	5.23±2.00	38	4.96±2.00	40	5.13
for_r	5.11±2.02	39	4.84±2.09	43	5.21
GM_lf	6.52±2.05	31	6.26±2.02	32	4.09
GM_lo	6.77±2.17	32	6.45±2.10	33	4.74
GM_lp	6.79±2.10	31	6.52±2.08	32	3.91
GM_rf	6.60±2.08	31	6.32±2.05	32	4.28
GM_ro	6.85±2.25	33	6.45±2.16	33	5.73
GM_rp	6.78±2.11	31	6.51±2.08	32	3.90
hip_l	6.76±2.54	38	6.30±2.48	39	6.88
hip_r	6.25±2.29	37	5.71±2.32	41	8.75
ins_l	6.80±2.48	37	6.33±2.48	39	6.92
ins_r	6.68±2.78	42	6.43±2.54	39	3.82
mtmp_l	6.38±2.26	35	6.01±2.23	37	5.75
mtmp_r	5.93±2.13	36	5.53±2.04	37	6.79
PuGP_l	7.77±3.08	40	7.51±2.84	38	3.36
PuGP_r	7.57±2.70	36	7.14±2.80	39	5.69
stem	5.41±1.86	34	4.84±1.87	39	10.58
Th_l	6.77±2.32	34	6.38±2.35	37	5.87
Th_r	6.66±2.18	33	6.27±2.20	35	5.95
tmp_l	6.56±2.06	31	6.27±2.02	32	4.36
tmp_r	6.60±2.14	32	6.32±2.10	33	4.27

[1] Estimates of K*p and K* r are represented as mean± S.D [ml/g/min].
[2]K*p: K* estimates obtained by MRI-segmented ROIs from K* map.
[3]K*r: K* estimates by TAC-based calculation.
[4]The meaning of these abbreviations is given in the list of abbreviations and in Table **1**. Abbreviations for the MRI segmented ROIs are given in the list of abbreviations.

evaluated by simulation. A tissue curve with a set of macro parameters [a=K1; b=K1 k3 and c= -(k2+k3)] as the mean values from ten controls was generated using model equation (Eq. 1). For each frame (each point of the TAC) a random Gaussian noise with variance ($\sigma^2(t_m)$) was added according to the equation 3 [27]:

$$\sigma^2(t_m) = \alpha \cdot \frac{C_i^*(t_m)}{\Delta t_i} \quad (3)$$

where t_m represents the middle point of a frame, Δt_i (min) is duration of the frame, $C_i^*(t_m)$ (Bq/g) is brain tissue tracer concentration for the frame "i" obtained at time t_m, and α is proportionality constant that determines the noise level in the measurement. A random number generator in Mathlab 7.1 was used to generate the Gaussian noise and it was added to the above mentioned generated TAC. The error variance from Eq. 3 with different values of α was used to generate 5000 TACs for all values of α except the value of 0.0. The values of α were 0.0 (noise free), 0.1, 0.2, 0.3, 0.4, 1.0, 2.0, and 4.0. The mean values of the macro parameters and K*

Table 3. Gray and white Matter Ratios (GM/WM Ratio) Comparison Between K* Map and Ki Map in 21 Subjects. Statistical Significance is Estimated by Paired-t Test[1]

		rf-ROI*	lf-ROI	rt-ROI	lt-ROI	rp-ROI	lp-ROI	ro-ROI	lo-ROI
Multilinear (K*)	Mean	1.259	1.222	1.257	1.230	1.434	1.424	1.078	1.106
	SD	0.293	0.259	0.253	0.280	0.399	0.369	0.076	0.098
Patlak (Ki)	Mean	1.086	1.036	1.139	1.078	1.195	1.177	0.997	1.015
	SD	0.144	0.119	0.175	0.149	0.162	0.155	0.112	0.105
	t-value	3.569	4.846	2.704	3.913	3.536	3.939	4.373	5.516
	p	0.0019	<0.0001	0.0137	0.0009	0.0021	0.0008	0.0003	<0.0001

***Abbreviations for brain regions**:
rf: right frontal
lf: left frontal
rt: right temporal
lt: left temporal
rp: right parietal
lp: left parietal
ro: right occipital
lo: left occipital
[1]No significant laterality

with associated SD were obtained from the least squares fitting of these TAC to Eq. 1 to assess the influence of errors in the TAC on the fitted parameters as well as on K*.

RESULTS

The volumes of the segmented ROIs used in different comparisons to obtain K* in selected brain region along with standard deviations (SD) are presented in Table **1**.

Comparison 1: K^*_s estimates by the less-invasive input function resulted on average in the values which are not significantly different from K^*_a estimates by the arterial input function, even though an underestimation of about 20% was observed in the peak of the normalized sinus TAC in the initial 20 minutes of the less-invasive input function (Nishizawa *et al*. 1998). In general the ratios across the brain in two subjects are very close to 1 (Fig **2A**), while in the third subject ratios are somewhat smaller than 1 (Fig. **2A**). An overestimation of the K^*_s/K^*_a ratio, but not significant, was observed, in the caudate nucleus and the brain stem (Fig. **2A**). These deviations are most likely statistical. However these did not have any significant influence on the overall ration for all three subjects, which is not significantly different from 1. The mean values of K^*_s/K^*_a ratios for all brain regions in each of three subjects were: 1.00±0.04 mL/g/min, 1.03±0.04 mL/g/min, and 0.92±0.14 mL/g/min. The overall mean of the K^*_s/K^*_a ratios for all three subjects was 0.98±0.10, the value not significantly different than 1 (t=1.74; p>0.08; df=96; one-sample two-tail t-test). The estimates of the the macro parameters (a, b and c; Eq. 1) were highly susceptible to the difference between the less-invasive and the arterial input functions (Fig. **2B**, **C**, **D**). The ratios between estimates obtained with the less-invasive and the arterial input for individual parameters, in contrast to the ratios of K*, were significantly greater than 1±0 (Figs. **2B**, **C**, **D**). The comparison of the ratios are shown in Figs. (**2**) (macro parameter a; Fig. **2B**); (macro parameter b; Fig. **2C**), and (macro parameter c; Fig. **2D**) for different brain regions and for each of subject's. There is an overestimation of all macro parameters with the less-invasive input function. The overestimation of these parameters presented by the ratios greater than 1 is substantially more variable between different subjects and different brain areas (Figs. **2B**, **2C** and **2D**) than is the case for K^*_s/K^*_a ratios (Fig. **2A**). The mean values of the ratios between these macro parameters obtained with the sinus-venous and arterial input functions were: a=2.21±0.84, b=1.99±0.59, and c=2.14±0.65. These values indicate that there is always overestimation of these macro parameters when less-invasive input function is used. This suggests that an accurate estimation of the individual parameters K1, K2 and k3 is not possible when using the less-invasive input function. However, the K*-values estimated from the macro parameters are in excellent agreement for data obtained with the two different input functions. The mean value of the K^*_s and K^*_a are 3.3±1.5 (μL/g/min) and 3.4±1.7 (μL/g/min), respectively. These values are not significantly different (p>0.7; df=170). The least squares fit of K^*_s as a function of K^*_a indicates very high correlation between two values; r^2=0.972 (df=170).

Comparison 2: Overall, K*p estimated by pixel-based calculation were on average approximately 5% smaller than K*r estimates by ROI-based calculation (Table **2**). When the difference in the individual ROIs is calculated it reveals that the underestimation of K*p was reasonably uniform in almost all brain structures. Some ROIs selected in relatively small regions with a substantial noise component resulted in a somewhat greater underestimation of K*p (e.g. amygdala). Mean, S.D. and coefficient of variation (COV) for K*p and K*r obtained in 21 normal controls are presented in Table **2**. K*r estimates clearly showed a smaller COV than the K*p estimates in most regions. This suggests that the use of K*r

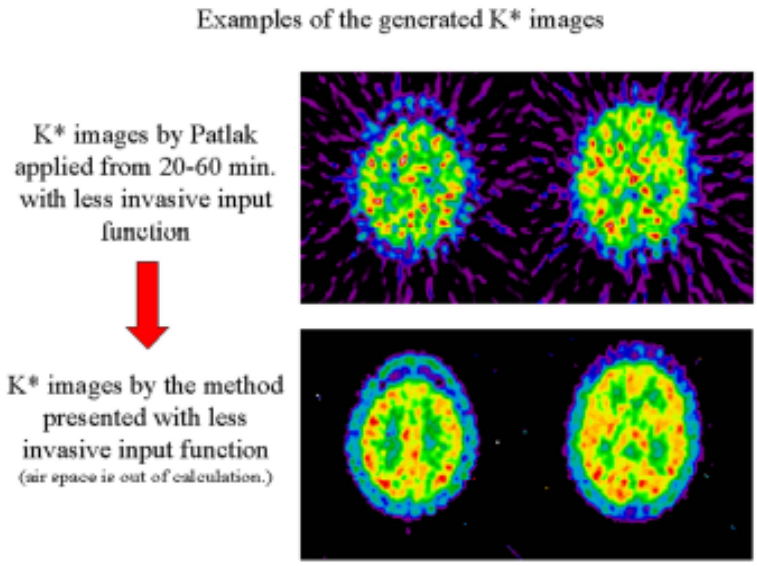

Fig. (3). Images represent trapping constant maps (K*i)obtained by the Patlak method (Eq. 2) (top row), and the linear solution with non-negative constraints, with BV adjustable (bottom row). These maps were generated from identical sets of dynamic PET data and sinus-venous input function. The exctracranial space was excluded in the calculations for bottom row images.

could be preferable for the statistical analysis of α-MTrp PET, if predefined regions could be considered for a particular study. There was no left to right significant difference ($p>0.05$; Repeated Measure ANOVA) in the trapping constant in this set of twenty one subjects.

Comparison 3: Examples of trapping constant images are presented in Fig. (**3**). Image 1 and Image 2 were generated from the kinetic linear solution for K* and the graphical approach for Ki, respectively. Cortical and sub cortical regions were distinctly visualized on the K* map in contrast to the patchy appearance of the Ki map.

As shown in Table **3**, the GM/WM (gray matter/white matter) ratios in the K* maps are significantly higher than those in the Ki-maps, as assessed by the paired-t test for four bilateral lobes of 21 normal subjects, when using the sinus-venous input function. Also, the pixel value distribution of GM ROIs resulted in smaller COVs for the K*-map than for the Ki-map. These findings suggest that for K* maps, gray matter is less likely to be excluded after applying a threshold to the parametric images, which is commonly observed in the statistical parametric software.

Percent coefficient of variation (COV) defined as SD divided with the estimated value and multiplied by 100 were also compared between those obtained by Eq. 1 and Eq. 2. The comparisons are graphically exemplified in Fig. (**4**). From the graph (comparison of two sets of values) it is can be observed that COVs for the solutions with Eq. 1are somewhat smaller (mean COV=0.22±0.06) than those for the Patlak fits (mean COV=0.23±0.05), but it is important to note that solution of Eq. 1 uses entire TAC while for the Patlak plot a decision must be made about which part of the curve one will use in the linear regression. The average values of K* estimated by Eqs. 1 and the Patlak fit are rather similar; (K*=6.5±0.6 and 6.2±0.6 μL/g/min, respectively).

Influence of Noise

As the noise in the TAC was increased the COV of K* was aslo increased (Fig. **5**), however the mean values of K* estimated from 5000 TAC are rather stable and varied from 7.04±0.11 (noise with α=0.01; Eq. 3) to 6.98±0.74 μL/g/min (noise with α=4, Eq. 3). In the contrast to a reasonable values of COV for K* estimates the COV for the individual model rate constants are substantial (see Fig. **5**). This simulation indicate that TACs even with the noise with α=4 (Eq. 3; [27]) gives K* estimates not significantly different from the values with low noise (α=0.01).

DISCUSSION

Comparison 1: The peak of the input function produced by bolus injection may be important in some parameter estimations, especially for the estimation of the initial distribution volume of the tracer, BV. However, whether the estimates of the parameters of interest for a tracer will be biased or not depends on the model structure and its mathematical description. For example, estimates of K* for deoxyglucose studies are not very sensitive to the peak of the input function [28]. It was also reported that K* for α-MTrp is insensitive to the peak of the input function when the Patlak method is used [17].

The data presented here also suggest that the bias in K* caused by underestimation of the peak in the initial 20 minutes of the input function is rather small, when Eq. 1 with non-negative constraints is used. This finding suggests that the less-invasive input function combined with the linear equation does not diminish the accuracy in estimating K* of α-MTrp, despite three factors affecting the peak of this input function obtained from PET images, namely: 1) tracer dispersion through the brain capillary vessels; 2) tracer extraction to the brain tissue; and 3) partial volume effect due to the limitation of the scanner's spatial resolution.

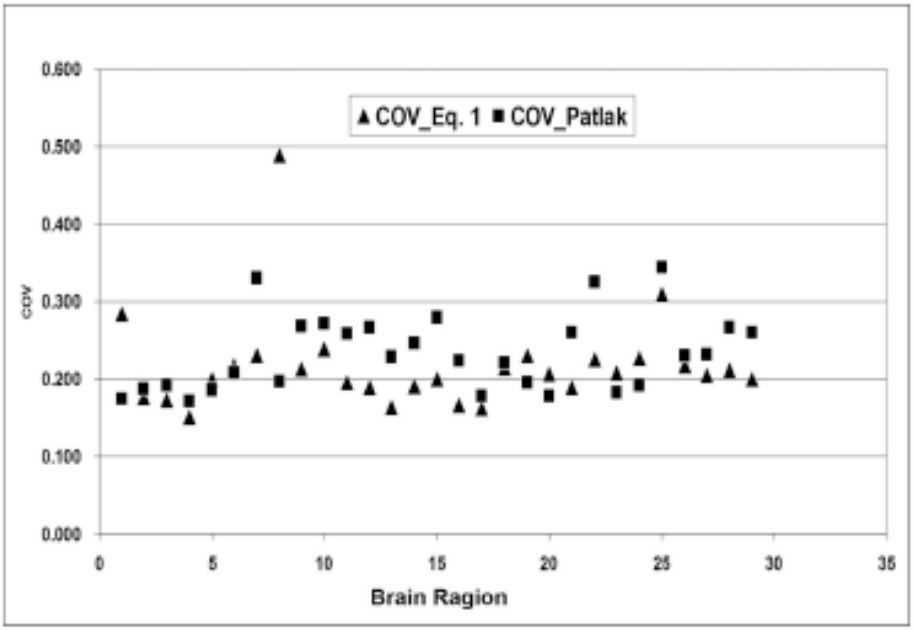

Fig. (4). A graph showing coefficient of variation (COV) for the K*i as a function of the brain region for the Patlak (Eq. 2) calculation and those for solution of Eq. 1. The brain regions are the same as those in Fig. (**2**).

Although the Blomqvist method has the potential to provide unbiased estimates of K1, the macro parameter estimates of a=K1, b=K1Ak3 and c=k2+k3, using the less-invasive input function, were substantially greater than those calculated with the arterial input function. This finding suggests that estimates of individual values of K1, k2 and k3 are very sensitive to the peak portion of the input function and that a substantial bias would be introduced to the estimates of the individual rate constants by using the less-invasive input function, as is the case with the macro parameters (Figs. **2B**, **C**, and **D**). However, the values of the parameter of interest in α-MTrp studies, namely K*, turned out not to be significantly biased and to be insensitive to the peak part of the input function. The high correlation (above 0.8) between different rate constants, as is in the case of FDG [29], is likely responsible for this.

Comparison 2: Ki estimates by the Patlak method for FDG studies do not show any systematic bias that might have been introduced by the noise in the data [30]. However, the noise in the dynamic PET data introduces some bias to the estimates of the individual kinetic constants, and this bias depends on the method used to calculate the parameters. For example, with the Logan graphical method, additive noise with zero mean in the tissue data results in a negative bias for the distribution volume of the receptor legends [31,32].

For the FDG model and the linear solution, the influence of noise on the value of K* has been explained by the trade-off relationship in the neighbouring frame times and error terms in the matrix equation, which are not independent [27,33].

A simulation study of FDG brain data has shown that K* was the least sensitive to noise among the kinetic parameters [34]. The data presented here indicate a similar trend: for α-MTrp studies, only a small difference and not significant was observed in the K* map with the less-invasive input function, and this underestimation was consistent and uniform over all brain structures investigated. This consistency in two kinds of K* estimates demonstrates that K*-maps are adequate to evaluate regional K*-values, despite the presence of a considerable noise component in the pixel-by-pixel calculation in the α-MTrp studies. It is always wise to perform an ROI-based kinetic calculation if a measurement in a small complex brain structure is of interest, like in the case of finding the epileptic focus in temporal lobe epilepsy [35].

Comparison 3: A significant enhancement of the grey to white matter contrast was obtained with the linearized method (Eq. 1), which would be consistent with a greater 5-HT synthesis in gray matter. Moreover, the statistical profile of the gray matter COV obtained from two types of trapping constant maps indicates that the linear solution gives smaller statistical variability in the gray matter than the Patlak method. Undeniably, the clear band-like appearance of the cortex accompanied by enhanced brain tissue contrast is more helpful for visual inspection than the patchy appearance extending over the whole brain volume.

Similar differences in appearance were observed in the trapping constant images when the Patlak and the linear methods using adjustable BV were compared. Because, in the case of α-MTrp, K* alone is the parameter of interest, one does not need to estimate the individual rate constants when a statistical parametric analysis package such as SPM 99 is used, because analyses are done on the normalized images [e.g. 36]. The greater contrasts in K* maps are of practical importance, because it eliminate possible white matter clusters which are of little interest in the study of 5-HT synthesis. As to the gray to white matter contrast, the α-MTrp studies with K* maps generated by the linear solution with non-negative constraints (Eq. 1) are more suitable than Ki maps obtained by the Patlak method. Simulations also sug-

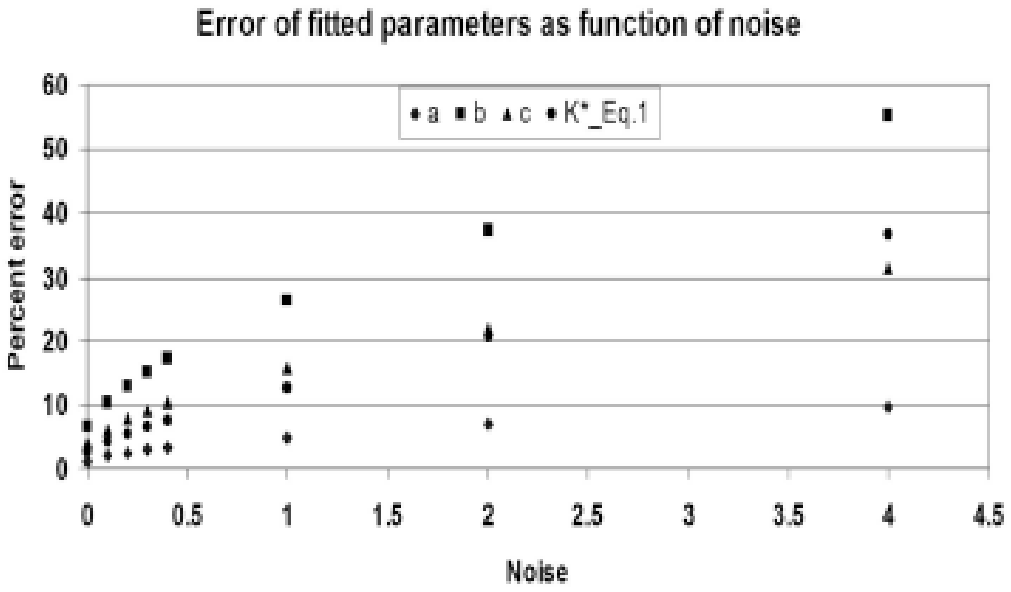

Fig. (5). A graphical presentation of the percent error in the model equation rate constants (Eq. 1) and the K* as a function of the noise defined by the α parameter in Eq. 3 [26]. These represent an average results from 5000 simulated curves.

gest that K* estimates with the linearized form of the model equation (Eq. 1) are rather insensitive to the noise in the TAC. A similar conclusions had been drawn for the FDG and FDOPA estimates of K* [29,37].

When radiopharmaceuticals with rather slow kinetics such as α-MTrp are used, there might be some practical difficulty in identifying the linear segment of the Patlak plot, and the apparent steady state assumption required for the use of the Patlak method might not be fully satisfied during the experimental period. This violation to the assumption of an apparent steady state required by the Patlak method may also imply the possible existence of an outlet from the irreversible compartment in the MTrp model, which will be the subject of future investigations.

The COV of the individual rate constants obtained in fitting Eq. 1 are substantial in comparison to the COV for K*, and vary between a few percent for K1 to over 90% for k3 (Fig. **5**). This observation is in an agreement with previous reports showing rather large COV for individual rate constant in α-MTrp model [11,12] as well as 2-Fluorodeoxyglucose [29] and fluoro DOPA [37,38] models in comparison for COV for K* which is in an order of 10% or less for actual TAC [36]. A similar conclusion is drown from simulation in which COVs in the individual parameters and K* were evaluated as a function of Gaussian noise (Fig. **5**).

CONCLUSION

The Blomqvist linear solution describing the three-compartment model has been successfully applied to generate improved images, in terms of tissue contrast and uniformity, of the trapping constant for α-MTrp in humans. This approach, combined with the use of the less-invasive input function, does not diminish the accuracy of the K*-maps. Compared to the graphical method (the Patlak method), the Blomqvist method has the advantage that it produces not only enhanced GM/WM contrast in the trapping constant map but also reduces noise in the gray matter. The resultant K* maps are more suitable and practical for visual inspection and further image manipulations such as statistical parametric mapping (e.g. SPM 99) in order to facilitate the detection of serotonergic abnormalities in the human brain.

ACKNOWLEDGEMENT

This work was supported by the Canadian Institute for Health Research (MOP-42438). We thank the Positron Emission Tomography and the Cyclotron-Radiochemistry Units of McGill University for their technical assistance. We would also like to thank Ms. Valerie-Ann Cherneski for editorial help.

ABBREVIATIONS

amy_l	=	Amygdala_left
amy_r	=	Amygdala_right
cing_l	=	Cingular cortex_left
cing_r	=	Cingular cortex_right
CN_l	=	Caudate_left
CN_r	=	Caudate_right
DG_l	=	Hypothalamus and other nucleus_left
DG_r	=	Hypothalamus and other nucleus_right
for_r	=	Fornix_right
for_l	=	Fornix_left
GM_lf	=	Gray matter_left frontal
GM_lo	=	Gray matter_left occipital
GM_lp	=	Gray matter_left parietal
GM_rf	=	Gray matter_right frontal
GM_ro	=	Gray matter_right occipital

GM_rp = Gray matter_right parietal

hip_l = Hippocampus_left

hip_r = Hippocampus_right

ins_r = Insula_right

ins_l = Insula_left

mtmp_l = Mesial temporal lobe_left

mtmp_r = Mesial temporal lobe_right

PuGP_l = Putamen and globus pallidus_left

PuGP_r = Putamen and globus pallidus_right

Th_l = Thalamus_left

Th_r = Thalamus_right

tmp_l = Lateral temporal lobe gray matter_left

tmp_r = Lateral temporal lobe gray matter_right

REFERENCES

[1] Jacobs BL, Azmitia EC. Structure and function of the brain serotonin system. Physiol Rev 1992; 72(1): 165-229.

[2] Van Praag HM. Anxiety and aggression as pacemakers of depression: a dimensional variation of the serotonin hypothesis of depression. In: Mendlewicz J, Racagni G, Brunello N, Eds. Current therapeutic approaches to panic and Other anxiety disorders. Basel: Karger 1994; pp. 144-50.

[3] Heninger GH, Indoleamine. The role of serotonin in clinical disorders. In: Loom FE, Kupfer DJ, Eds. Psychopharmacology: the fourth generation of progress. New York: Raven Press 1995; pp. 471-82.

[4] Brewerton TD. Toward a unified theory of serotonin dysregulation in eating and related disorders. Psychoneuroendocrinology 1995; 20(6): 561-90.

[5] Nelson N. Presynaptic events involved in neurotransmission. J Physiol (Paris) 1993; 87: 171-8.

[6] Diksic M, Tohyama Y, Takada A. Brain net unidirectional uptake of alpha-[14C]methyl-L-tryptophan (alpha-MTrp) and its correlation with regional serotonin synthesis, tryptophan incorporation into proteins, and permeability surface area products of tryptophan and alpha-MTrp. Neurochem Res 2000; 25: 1537-46.

[7] Diksic M, Nagahiro S, Sourkes TL, Yamamoto YL. A new method to measure brain serotonin synthesis *in vivo*. I. Theory and basic data for a biological model. J Cereb Blood Flow Metab 1990; 10(1): 1-12.

[8] Diksic M. Labelled alpha-methyl-L-tryptophan as a tracer for the study of the brain serotonergic system. J Psychiatr Neurosci 2001; 26: 293-303.

[9] Diksic M, Young SN. Study of the brain serotonergic system with labeled alpha-methyl-L-tryptophan. J Neurochem 2001; 78: 1185-200.

[10] Tohyama Y, Yamane F, Merid MF, Diksic M. Effects of selective 5-HT1A receptor antagonists on regional serotonin synthesis in the rat brain: an autoradiographic study with alpha-[14C]methyl-L-tryptophan. Eur Neuropsychopharmacol 2001; 11: 193-202.

[11] Nishizawa S, Benkelfat C, Young SN, *et al*. Differences between males and females in rates of serotonin synthesis in human brain. Proc Natl Acad Sci USA 1997; 94: 5308-13.

[12] Muzik O, Chugani DC, Chakraborty P, Mangner T, Chugani HT. Analysis of [C-11]alpha-methyl-tryptophan kinetics for the estimation of serotonin synthesis rate *in vivo*. J Cereb Blood Flow Metab 1997; 17: 659-69.

[13] Leyton M, Okazawa H, Diksic M, *et al*. Brain Regional alpha-[11C]methyl-L-tryptophan trapping in impulsive subjects with borderline personality disorder. Am J Psychiatry 2001; 158: 775-82.

[14] Nishikawa M, Kumakura Y, Young SN, *et al*. Increasing blood oxygen increases an index of 5-HT synthesis in human brain as measured using alpha-[(11)C]methyl-L-tryptophan and positron emission tomography. Neurochem Int 2005; 47(8): 556-64.

[15] Sakai Y, Nishikawa M, Leyton M, Benkelfat C, Young SN, Diksic M. Cortical trapping of alpha-[(11)C]methyl-l-tryptophan, an index of serotonin synthesis, is lower in females than males. Neuroimage 2006; 33(3): 815-24.

[16] Chugani DC, Muzik O. Alpha[C-11]methyl-L-tryptophan PET maps brain serotonin synthesis and kynurenine pathway metabolism. J Cereb Blood Flow Metab 2000; 20(1): 2-9.

[17] Nishizawa S, Leyton M, Okazawa H, Benkelfat C, Mzengeza S, Diksic M. Validation of a less-invasive method for measurement of serotonin synthesis rate with alpha-[11C]methyl-tryptophan. J Cereb Blood Flow Metab 1998; 18: 1121-9.

[18] Okazawa H, Leyton M, Benkelfat C, Mzengeza S, Diksic M. Statistical mapping analysis of serotonin synthesis images generated in healthy volunteers using positron-emission tomography and alpha-[11C]methyl-L-tryptophan. J Psychiatr Neurosci 2000; 25: 359-70.

[19] Blomqvist G. On the construction of functional maps in positron emission tomography. J Cereb Blood Flow Metab 1984; 4(4): 629-32.

[20] Mzengeza S, Venkatachalam TK, Diksic M. Asymmetric radiosynthesis of alpha-[11C]methyl-L-tryptophan for PET studies. Nucl Med Biol 1995; 22: 303-7.

[21] Collins DL, Holmes CJ, Peters TM, Evans AC. Automatic 3-D model-based neuroanatomical segmentation. Hum Brain Mapp 1995; 3: 190-208.

[22] Collins DL, Evans AC. ANIMAL: Validation and applications of nonlinear registration-based segmentation. Intern J Pattern Recogn Artif Intell 1997; 11: 1271-94.

[23] Collins DL, Zijdenbos AP, Barre WFC, Evans AC. ANIMAL+INSECT: Improved Cortical Structure Segmentation. Kuba A, Samal A, Todd-pokrope KA, Eds. Springer-Verlag: Berlin Heidelberg 1999; pp.210-23.

[24] Collins DL, Neelin P, Peters TM, Evans AC. Automatic 3D intersubject registration of MR volumetric data in standardized talairach space. J Comp Assist Tomog 1994; 18(2): 192-205.

[25] Diksic M, Nagahiro S, Chaly T, Sourkes TL, Yamamoto YL, Feindel W. Serotonin synthesis rate measured in living dog brain by positron emission tomography. J Neurochem 1991; 56(1): 153-62.

[26] Patlak CS, Blasberg RG, Fenstermacher JD. Graphical evaluation of blood-to-brain transfer constants from multiple-timeuptake data. J Cereb Blood Flow Metab 1983; 3: 1-7.

[27] Feng D, Huang S-C, Wang Z, Ho D. An unbiased parametric imaging algorithm for nonuniformly sampled biomedical system parameter estimation. IEEE Trans Med Imaging 1996; 15: 512-8.

[28] Kato A, Menon D, Diksic M, Yamamoto YL. Influence of the input function on the calculation of the local cerebral metabolic rate for glucose in the deoxyglucose method. J Cereb Blood Flow Metab 1984; 4: 41-6.

[29] Evans AC, Diksic M, Yamamoto YL, *et al*. Effect of vascular activity in the determination of rate constants for the uptake of 18F-labeled 2-fluoro-2-deoxy-D-glucose: error analysis and normal values in older subjects. J Cereb Blood Flow Metab 1986; 6: 724-38.

[30] Feng D, Ho D, Chen K, *et al*. An evaluation of the algorithms for determining local cerebral metabolic rates of glucose using positron emission tomography dynamic data. IEEE Trans Med Imaging 1995; 14: 697-710.

[31] Slifstein M, Laruelle M. Effects of statistical noise on graphic analysis of PET neuroreceptor studies. J Nucl Med 2000; 41: 2083-8.

[32] Abi-Dargham A, Martinez D, Mawlawi O, *et al*. Measurement of striatal and extrastriatal dopamine D1 receptor binding potential with [11C]NNC 112 in humans: validation and reproducibility. J Cereb Blood Flow Metab 2000; 20(2): 225-43.

[33] Feng D, Wang Z, Huang S-C. A study on statistically reliable and computationally efficient algorithms for the measurement of local cerebral blood flow with positron emission tomography. IEEE Trans Med Imaging 1993; 12: 182-8.

[34] Thie JA, Smith GT, Hubner KF. Linear least squares compartmental-model-independent parameter identification in PET. IEEE Trans Med Imaging 1997; 16: 11-6.

[35] Natsume J, Kumakura Y, Bernasconi N, *et al*. α-[^{11}C]MTrp and [^{18}F]FDG hippocampal uptake are negatively correlated in patients with temporal lobe epilepsy. Neurology 2003; 60: 756-61.

[36] Okazawa H, Diksic M. Image generation of serotonin synthesis rates using alpha-methyltryptophan and PET. J Comput Assist Tomogr 1998; 22(5): 777-85.

[37] Huang SC, Yu DC, Barrio JR, *et al*. Kinetics and modeling of L-6-[18F]fluoro-dopa in human positron emission tomographic studies. J Cereb Blood Flow Metab 1991; 11(6): 898-13.

[38] Kuwabara H, Cumming P, Reith J, *et al*. Human striatal L-dopa decarboxylase activity estimated *in vivo* using 6-[18F]fluoro-dopa and positron emission tomography: error analysis and application to normal subjects. J Cereb Blood Flow Metab 1993; 13(1): 43-56.

Received: January 17, 2011 Revised: April 18, 2011 Accepted: April 18, 2011